PAPER

High-dimensional generalizations of the Lorenz system and implications for predictability

IOP Publishing Physica Scripta
Phys. Scr. 95 (2020) 085209 (14pp) https://doi.org/10.1088/1402-4896/ab9d3e

High-dimensional generalizations of the Lorenz system and implications for predictability

Sungju Moon[1], Jaemyeong Mango Seo[2] and Jong-Jin Baik[1]

[1] School of Earth and Environmental Sciences, Seoul National University, Seoul 08826, Republic of Korea
[2] Max Planck Institute for Meteorology, Bundesstraße 53, 20146 Hamburg, Germany

E-mail: jjbaik@snu.ac.kr

Received 17 April 2020, revised 3 June 2020
Accepted for publication 16 June 2020
Published 25 June 2020

Abstract

A set of $(3N)$- and $(3N + 2)$-dimensional ordinary differential equation systems for any positive integer N are newly derived as high-dimensional extensions of the three-dimensional Lorenz system, and their numerical solutions are analyzed using periodicity diagrams, bifurcation diagrams, solution trajectories, and initial condition experiments. Higher-dimensional Lorenz systems extended in this manner can be considered to be closer to the original governing equations describing Rayleigh-Bénard convection in the sense that they incorporate smaller-scale motions. This study focuses on how the solution characteristics react to incremental changes in the dimension of the Lorenz system. By plotting periodicity diagrams in dimension-parameter spaces, it is shown that the parameter ranges in which the systems have chaotic solutions tend to diminish with increasing dimensions. On the other hand, for particular parameter choices that result in chaotic solutions across many dimensions, having a higher dimension does not always result in a faster or slower initial error growth. Possible implications of these results are discussed in the context of predictability.

Keywords: high-dimensional Lorenz system, chaos, initial conditions, predictability

(Some figures may appear in colour only in the online journal)

1. Introduction

As one of the first systems known to feature a strange attractor [1], the three-dimensional Lorenz system [2] continues to be an important topic of investigation in nonlinear dynamics and chaos theory. The three-dimensional Lorenz system consists of the following ordinary differential equations (ODE) in three variables, X, Y, and Z:

$$\dot{X} = -\sigma X + \sigma Y, \tag{1}$$

$$\dot{Y} = -XZ + rX - Y, \tag{2}$$

$$\dot{Z} = XY - bZ, \tag{3}$$

where the dot above each variable denotes the derivative with respect to time τ. The three parameters r, σ, and b are referred to as the Rayleigh parameter, the Prandtl number, and a geometric parameter, respectively. Considering the relative simplicity of (1)–(3) in form, a stark contrast against their solutions' complex and seemingly unpredictable behavior, there has remained continual interest in extensions of this system to higher dimensions and the changes such extensions bring about [3]. Motives vary when it comes to why a particular high-dimensional Lorenz system is in demand. From a physical point of view, high-dimensional systems can make for a more realistic model either because they include more Fourier modes in the derivation [4–6] or because additional elements of the physical reality are considered [7–13]. There is also a possibility of discovering an entirely new phenomenon exclusive to high-dimensional systems such as hyperchaos [14–18].

The aforementioned reasons have led to two distinct but not exclusive approaches to generalizing the original Lorenz system into higher dimensions [3]. First, one can include additional physical processes at the governing equations

stage, thereby obtaining ODE systems with more variables and parameters [7–11, 17, 19]. Second, one can include additional modes when truncating the Fourier series in the derivation of ODE systems, thereby bringing the ODE systems closer to the untruncated PDE system. The present study is concerned with generalizing the Lorenz system following the latter approach. The derivation in appendix shows that such generalizations lead to high-dimensional Lorenz systems consisting of $(3N)$ or $(3N + 2)$ equations for any positive integer N.

The Lorenz system as a model of thermal convection retains many of the qualitative features central to the emergence of turbulence and chaotic fluid motions associated with changes in parameters [20]. In particular, it is well known that parameter r plays an important role in regulating whether the solution should be chaotic or non-chaotic [2, 20–22]. In the three-dimensional Lorenz system with otherwise standard parameter values $\sigma = 10$ and $b = 8/3$, heteroclinic bifurcation occurs when r is raised beyond a certain critical value, giving birth to a strange attractor [1, 21]. High-dimensional systems are generally considered to be more resistant to chaos than low-dimensional systems [3]. Particularly for r, the critical Rayleigh parameter was found to increase in a five-dimensional Lorenz system derived from the inclusion of one additional mode in each Fourier series expansion [5] and to slightly decrease in the six-dimensional system derived in the same manner [23]. A comparative study of the high-dimensional Lorenz systems up to 11 dimensions [6] suggests an overall increase in the critical r in response to raising the dimension in this way. It remains to be seen whether the critical r continues to increase with further extensions of the Lorenz system to even higher dimensions.

In addition to r, one can also vary σ [24]. Exploring the σ-r parameter space allows one to consider both σ and r simultaneously, which has been done extensively for the original Lorenz system [17, 18, 25–29]. Plotted in the σ-r parameter space, elaborate patterns have been reported for the numerical solutions of the three-dimensional system including the so-called 'onionlike structure' consisting of alternating regimes of chaos and periodicity in high-dimensional Lorenz systems [6, 27]. In [6], the onionlike structure was reported to disappear starting at dimension 6, coinciding with the expansion of periodic regions in the σ-r parameter space.

This study aims to analyze the $(3N)$- and $(3N + 2)$-dimensional systems that generalize the high-dimensional Lorenz systems studied in [6], with a particular focus on examining whether the observed behavior of high-dimensional Lorenz systems continues over a wide range of dimensions. Section 2 introduces the generalizations. Section 3 studies the stability of the newly derived systems after linearization, and section 4 analyzes the numerically obtained solutions, examining their periodicity patterns in dimension-parameter spaces as well as their bifurcation structures and solution trajectories. We then shift our attention to the question of predictability and discuss possible implications in section 5. This study examines two notions of predictability applicable to the observed solution characteristics in the high-dimensional Lorenz systems: first, the likelihood of encountering chaos given a parameter combination and second, how quickly solutions with a tiny difference in initial conditions deviate from one another. Initial condition experiments are carried out for a broad selection of dimension-parameter combinations to explore if there are patterns to how the second notion of predictability responds to changes in dimension and parameters. A summary and discussion are given in section 6.

2. The (3*N*)- and (3*N*+2)-dimensional generalizations

As generalizations of the three variables X, Y, and Z in the three-dimensional Lorenz system, we introduce the kth variables, denoted by X_k, Y_k, and Z_k, respectively, so that the left-hand-side of each equation comprising the generalized system is $\dot{X}_k$, $\dot{Y}_k$ or $\dot{Z}_k$. Let N be the number of equations with $\dot{X}_k$ on the left-hand-side and M be the number of $\dot{Y}_k$ equations or, equivalently, the number of $\dot{Z}_k$ equations. Together, these equations form an $(N + 2M)$-dimensional system, which becomes either a $(3N)$-dimensional or a $(3N + 2)$-dimensional generalized Lorenz system depending on the choice of M and N.

2.1. The P_k- and Q_k-sets for nonlinear terms

For each of the $\dot{Y}_k$ equations, define a set P_k consisting of the index pairs $(i, j) \subset \mathbb{Z}^2$, $0 < i \leqslant N$, $0 < j \leqslant M$, such that one of the following conditions is satisfied: $i + j = k$, $j - i = k - 1$, or $i - j = k$. The sign function $\mathscr{S}_Y$ for the X_iZ_j terms in the $\dot{Y}_k$ equation is defined by

$$\mathscr{S}_Y = \begin{cases} -1 & \text{if } j - i = k - 1, \\ 1 & \text{otherwise.} \end{cases} \tag{4}$$

Likewise, for each of the $\dot{Z}_k$ equations, define a set Q_k consisting of the index pairs $(i, j) \subset \mathbb{Z}^2$, $0 < i \leqslant N$, $0 < j \leqslant M$ such that one of the following conditions is satisfied: $j + i = k + 1$ or $|j - i| = k$. The sign function $\mathscr{S}_Z$ for the X_iY_j terms in the $\dot{Z}_k$ equation is defined by

$$\mathscr{S}_Z = \begin{cases} -1 & \text{if } |j - i| = k, \\ 1 & \text{otherwise.} \end{cases} \tag{5}$$

2.2. The (3*N*)- and (3*N*+2)-dimensional systems

The $(3N)$-dimensional system consists of $N = M$ variables for each variable type. For any given positive integer $k \leqslant N$,

$$\dot{X}_k = -d_k\sigma X_k + \frac{\sigma}{d_k}Y_k, \tag{6}$$

$$\dot{Y}_k = rX_k - d_kY_k + \sum_{(i,j)\in P_k} (jX_iZ_j\mathscr{S}_Y), \tag{7}$$

$$\dot{Z}_k = -k^2bZ_k + \sum_{(i,j)\in Q_k} (kX_iY_j\mathscr{S}_Z), \tag{8}$$

where the indices i and j are positive integers. The variables consisting of nonlinear products (such as X_iZ_j or X_iY_j) are chosen by the indices belonging to P_k or Q_k.

The $(3N + 2)$-dimensional system consists of N number of X variables and $N + 1 = M$ number of Y and Z variables each. For $k \leqslant N$,

$$\dot{X}_k = -d_k \sigma X_k + \frac{\sigma}{d_k} Y_k, \tag{9}$$

$$\dot{Y}_k = rX_k - d_k Y_k + \sum_{(i,j)\in P_k} (jX_i Z_j \mathscr{S}_Y), \tag{10}$$

$$\dot{Z}_k = -k^2 b Z_k + \sum_{(i,j)\in Q_k} (kX_i Y_j \mathscr{S}_Z). \tag{11}$$

For $k = M = N + 1$,

$$\dot{Y}_k = -d_k Y_k + \sum_{(i,j)\in P_k} (jX_i Z_j \mathscr{S}_Y), \tag{12}$$

$$\dot{Z}_k = -k^2 b Z_k + \sum_{(i,j)\in Q_k} (kX_i Y_j \mathscr{S}_Z). \tag{13}$$

3. Linear stability analysis

For the $(3N)$-dimensional systems, linearization of the system can be achieved by applying infinitesimal perturbations $\mathbf{X}'$ of the variables at a point $\mathbf{X}_0 = (X_{1,0}, Y_{1,0}, Z_{1,0}, \ldots, X_{N,0}, Y_{N,0}, Z_{N,0})$ in the $(3N)$-dimensional space. In matrix notation,

$$\frac{d}{dt}\mathbf{X}' = \mathbf{M}\mathbf{X}' = \sum_{i,k\leqslant N} (\mathbf{N}_{i,k} + \mathbf{L}_k)\mathbf{X}', \tag{14}$$

where $\mathbf{M}$ is the $3N \times 3N$ matrix consisting of the coefficients of the linearized system. The $3N \times 3N$ matrices, $\mathbf{N}_{i,k}$ and $\mathbf{L}_k$, are given for each $k \leqslant N$ and $i \leqslant N$ by

$$\mathbf{N}_{i,k} = \begin{array}{c} \\ \text{row } (3k-1) \\ \\ \text{row } (3k) \end{array} \begin{array}{c} \text{column } (3i-2) \\ \begin{pmatrix} (k-i)Z_{k-i,0} \\ +(i-k)Z_{i-k,0} \\ -(k+i-1)Z_{k+i-1,0} \end{pmatrix} \\ k\begin{pmatrix} Y_{k+1-i,0} \\ -Y_{k+i,0} - Y_{i-k,0} \end{pmatrix} \end{array} \begin{array}{c} \text{column } (3i-1) \\ 0 \\ k\begin{pmatrix} X_{k+1-i,0} \\ -X_{k+i,0} - X_{i-k,0} \end{pmatrix} \end{array} \begin{array}{c} \text{column } (3i) \\ i\begin{pmatrix} X_{k-i,0} \\ +X_{k+i,0} \\ -X_{i+1-k,0} \end{pmatrix} \\ 0 \end{array} \tag{15}$$

and

$$\mathbf{L}_k = \begin{array}{r} \\ \text{row } (3k-2) \\ \text{row } (3k-1) \\ \text{row } (3k) \end{array} \begin{array}{ccc} \text{column } (3k-2) & \text{column } (3k-1) & \text{column } (3k) \\ -d_k\sigma & \frac{\sigma}{d_k} & 0 \\ r & -d_k & 0 \\ 0 & 0 & -k^2 b \end{array} \tag{16}$$

with all other entries zeroed out. Then the sign of the largest of the real parts of eigenvalues of matrix $\mathbf{M}$ can be used for stability analysis. Consider, for example, the point $\mathbf{X}^*$ given by $(X_k, Y_k, Z_k) = (\sqrt{b(r-1)}, \sqrt{b(r-1)}, r-1)$ for all $k \leqslant N$. For the three-dimensional system, this point is in fact a nontrivial fixed point which loses stability through Hopf bifurcation as the largest of the real parts of the eigenvalues of $\mathbf{M}$ becomes negative. For systems with dimensions greater than three, however, this point lies somewhere near one of the fixed points. The changing stability at this point, while not indicative of a global bifurcation, can give us a clue regarding the direction in which changing parameters or dimension affects the system.

In figure 1(a), it is apparent that the stability curve moves northward in the σ-r space if the dimension is raised. From this, one can expect the value of r at which the solution becomes unstable around the point $\mathbf{X}^*$ to increase with increasing the dimension of the system. Likewise, we can see in figure 1(b) that given the traditional value of $\sigma = 10$, the r value beyond which the solution becomes unstable around the point $\mathbf{X}^*$ rapidly increases with dimension, while given a higher σ, the steepness of this incline becomes somewhat less extreme. This suggests that there is a greater chance of the system remaining unstable in higher-dimensional systems if σ is raised from 10 to 50. Similarly, figure 1(c) suggests that the solution is still unstable around $\mathbf{X}^*$ in higher-dimensional systems if r is raised alongside the dimension of the system. It must be emphasized that the above statements are made based on the local stability of a rather arbitrarily chosen point $\mathbf{X}^*$. For this reason, any discussion about specific features of the stability curves, such as the dip in the critical r from dimension 6 to dimension 12 in figure 1(b) is necessarily limited in scope by that specific point in the phase space and is likely irrelevant to the global bifurcation structure of the system.

A more comprehensive approach would be to look at the system's stability around all nontrivial fixed points that exist in the system. It is, however, unlikely that general closed-form solutions are available for all fixed points in systems with dimension greater than five as such a task likely requires solving polynomial equations of degree greater than five. Furthermore, the above analysis only applies to $(3N)$-dimensional systems but not $(3N + 2)$-dimensional systems. Given these difficulties, we opt for a numerical approach hereafter.

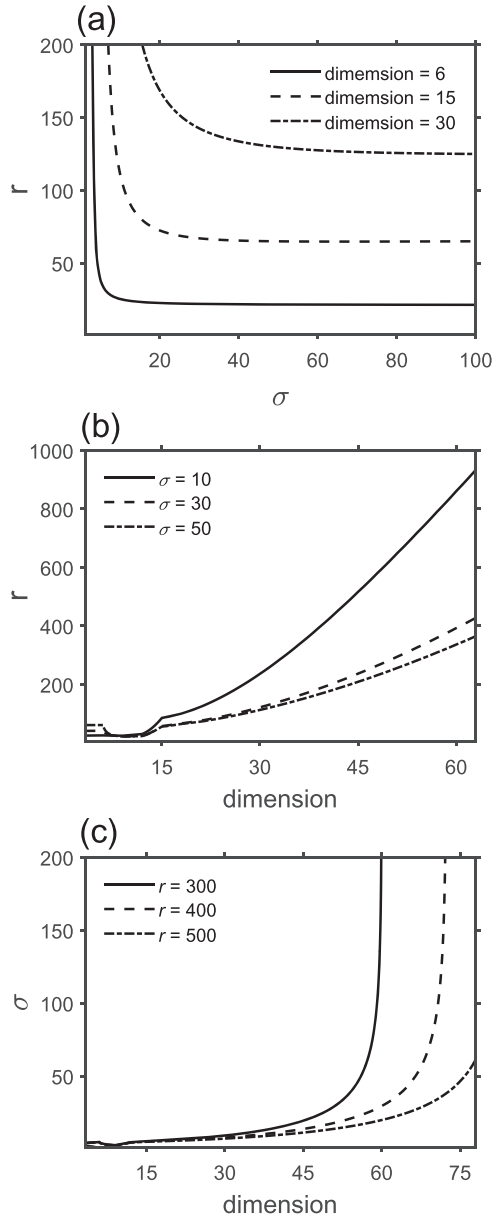

Figure 1. Curves indicating local stability change at the point $(X_i, Y_i, Z_i) = (\sqrt{b(r-1)}, \sqrt{b(r-1)}, r-1)$ for all $i \leqslant N$ for the generalized Lorenz system of dimension $3N$ in (a) the σ-r parameter space for dimensions 6, 15, and 30, (b) the dimension-r space for $\sigma = 10$, 30, and 50, and (c) the dimension-σ space for $r = 300$, 400, and 500.

4. Numerical results: chaos in dimension-parameter spaces

In the following, the numerical solutions are obtained using the fourth-order Runge-Kutta method with time resolution $\Delta\tau = 10^{-4}$. Unless otherwise specified, the initial conditions are given by $(X_1, Y_1, Z_1, \ldots) = (1, 0, 0, \ldots)$ and the parameter $b = 8/3$ is fixed.

For periodicity diagrams in dimension-parameter spaces (figure 2), we use the time series of the numerically obtained solutions for variable Z_1 following [27] and [19]. To briefly explain periodicity diagrams, note that periodic solutions will have a finite number of peaks forming a pattern that repeats itself. Our algorithm flags the first peak of this pattern after $\tau = 200$ and counts the number of subsequent local maxima up to and including the first repetition of the flagged, whose magnitude is equal to that of the flagged within the tolerance given by 0.1% the magnitude of the flagged. Hereafter, the number of peaks counted in this way is referred to as period number p and such a solution is said to be of p-periodic. If the solution is chaotic, however, there is necessarily no repeated pattern of peaks and troughs; hence, we only count the number of peaks up to period 8 and consider any solution with period number $\geqslant 8$ to be chaotic following [13]. Those rare cases in which the solution is truly 8-periodic but not chaotic can usually be detected by also checking the trajectories of their numerical solutions. Lastly, if the solution is stable after $\tau = 200$, its trajectory converges to one of the fixed points and there is no peak in the time series. In this case, 0 is assigned to the period number. In periodicity diagrams in figure 2, each period number is assigned a color: white for chaos, black for stability, and other colors for different period numbers. Accompanying figure 2 is figure 3 which provides trajectories of the numerical solutions in phase spaces corresponding to specific parameter combinations. Insofar as the authors' knowledge, this is the first time dimension is used as one of the axes in a periodicity diagram for detecting the bifurcation structure of a nonlinear system.

The emergence of chaos as the Rayleigh parameter crosses the critical threshold at $r \sim 24.06$ in the three-dimensional Lorenz system with standard values for $\sigma = 10$ and $b = 8/3$ is well documented [2, 21, 22, 28] and is also seen in figure 2(a) at $r = 25$ due to having the resolution of $\Delta r = 1$. The high-dimensional Lorenz systems are also known to be more resistant to chaos [3, 6] in the sense that the critical Rayleigh parameter for emergence of chaos increases with the dimension of the system. In figure 2(a), it is shown that this delay of emergence of chaos rapidly intensifies with dimension in such a way that at dimension 14, there is no unstable region captured in the r window between $r = 0$ and $r = 1000$. Even with $\sigma = 50$, for which it is known that unstable solutions are captured more across different values of r [6], a rapid increase in the critical r with dimension is still seen, albeit with more widespread chaos overall (figure 2(b)).

Figures 2(c) and (d) show the periodicity structures in the dimension-σ space for different r values, $r = 400$ and $r = 500$. The motivation for plotting these periodicity diagrams comes from the observed changes in the σ-r periodicity diagrams going from three to higher dimensions. In [6], it is reported that the onionlike structure [27] from the three-dimensional Lorenz system consisting of alternating bands of chaos and periodicity within the unstable region of the σ-r periodicity diagram diminishes for dimensions beyond 5, save for the first major columnar band of chaos standing vertically for $r \gtrsim 24$ whose width is contained within the parameter domain $\sigma \in [0, 100]$. A periodicity diagram in the dimension-σ space with a fixed r value, therefore, captures the evolution of the width of this *first band of chaos* in the σ-r space and any additional secondary bands of chaos that may emerge at higher σ values.

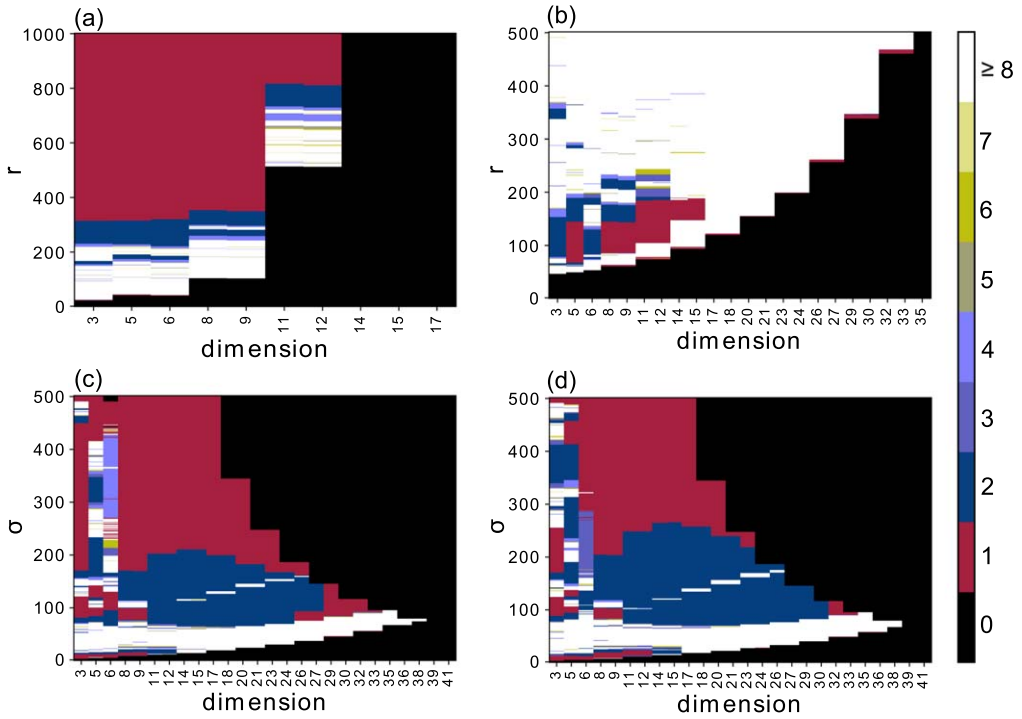

Figure 2. Periodicity diagrams in the dimension-r space with (a) $\sigma = 10$ and (b) $\sigma = 50$. Periodicity diagrams in the dimension-σ space with (c) $r = 400$ and (d) $r = 500$.

Figures 2(c) and (d) feature a few shared characteristics. First, there is the region of period 2 (dark blue) that is mostly bounded either by the first band of chaos (thick white band at the bottom with an uptick towards higher dimensions) or by regions of period 1 (dark red area) within the unstable region. Second, the periodicity diagrams exhibit a step function-like structure comprising some secondary bands of chaos (white) for dimensions ranging from 14 to 26 in figure 2(c) and starting at even lower dimensions in figure 2(d), contained within the region of period 2. Notice, for high dimensions, the $(3N + 2)$-dimensional systems behave in lockstep with the $3(N + 1)$-dimensional systems that come next. The trajectories for the chaotic solutions that make up this step function-like structure feature two additional loops as seen in figure 3(a) resulting from the unstable manifold's coiling around the Z_1-axis as shown in figure 3(b), which is characteristic of the chaotic trajectories belonging to the second band of chaos [6]. Neither the first nor the secondary bands of chaos go on forever with rising dimensions, however, which leads to our third observation: instability vanishes beyond a certain threshold dimension for all σ values shown in figures 2(c) and (d).

In order to see the evolution of periodicity with dimension more clearly, bifurcation diagrams as a function of dimension are plotted in figure 4 using the peak values of Z_1 in the numerically obtained time series of solutions. Figure 4(a) corresponds to cutting across the first chaotic band shown in figure 2(c) near the band's core at $\sigma = 40$. In this case, chaos is maintained throughout the dimension range until the instability vanishes at dimension 29, although the Z_1-peaks split into two groups starting at dimension 20. For systems with dimensions <20, the chaotic trajectories fill in the gaps around the nontrivial fixed points near the centers of the butterfly wings of the attractor as shown in figure 3(c). For this reason, the Z_1-peaks in figure 4(a) appear as one lump of points scattered about over a range of Z_1-values when dimension is <20. In higher-dimensional systems, on the other hand, there is a split amongst the Z_1-peaks. With this split, the trajectories around the nontrivial fixed points maintain a certain distance from the center, resulting in the smaller Z_1-peaks being distinguishable from the group of Z_1-peaks with larger magnitudes. This grouping of Z_1-peaks in chaotic solutions is also seen when $\sigma = 70$ (see figures 4(b) and 3(d)), although here the two lumps of Z_1-peaks come out of the two Z_1-peaks in periodic solutions at lower dimensions. When σ is even higher at 100, periodic solutions dominate for systems with dimensions greater than 9. Most of the 2-periodic solutions form symmetric loops (Figure 3(f)) while some asymmetric 2-periodic solutions are also observed (figure 3(e)).

Together with the bifurcation diagrams in figure 4, the periodicity diagrams in figure 2 suggest that, all else being equal, raising the dimension of the Lorenz system diminishes the region of instability. Even for a parameter window that captures chaos in an extended range of dimensions such as $\sigma \in [0, 100]$ in figure 2(c) and $r \in [400, 500]$ in figure 2(b), chaos becomes less likely at higher dimensions and eventually disappears entirely when the dimension of the system is high enough.

5. Predictability and sensitivity to initial conditions

Because it is thought that the chaotic solutions of the Lorenz system represent the effects of nonlinearity in the atmosphere,

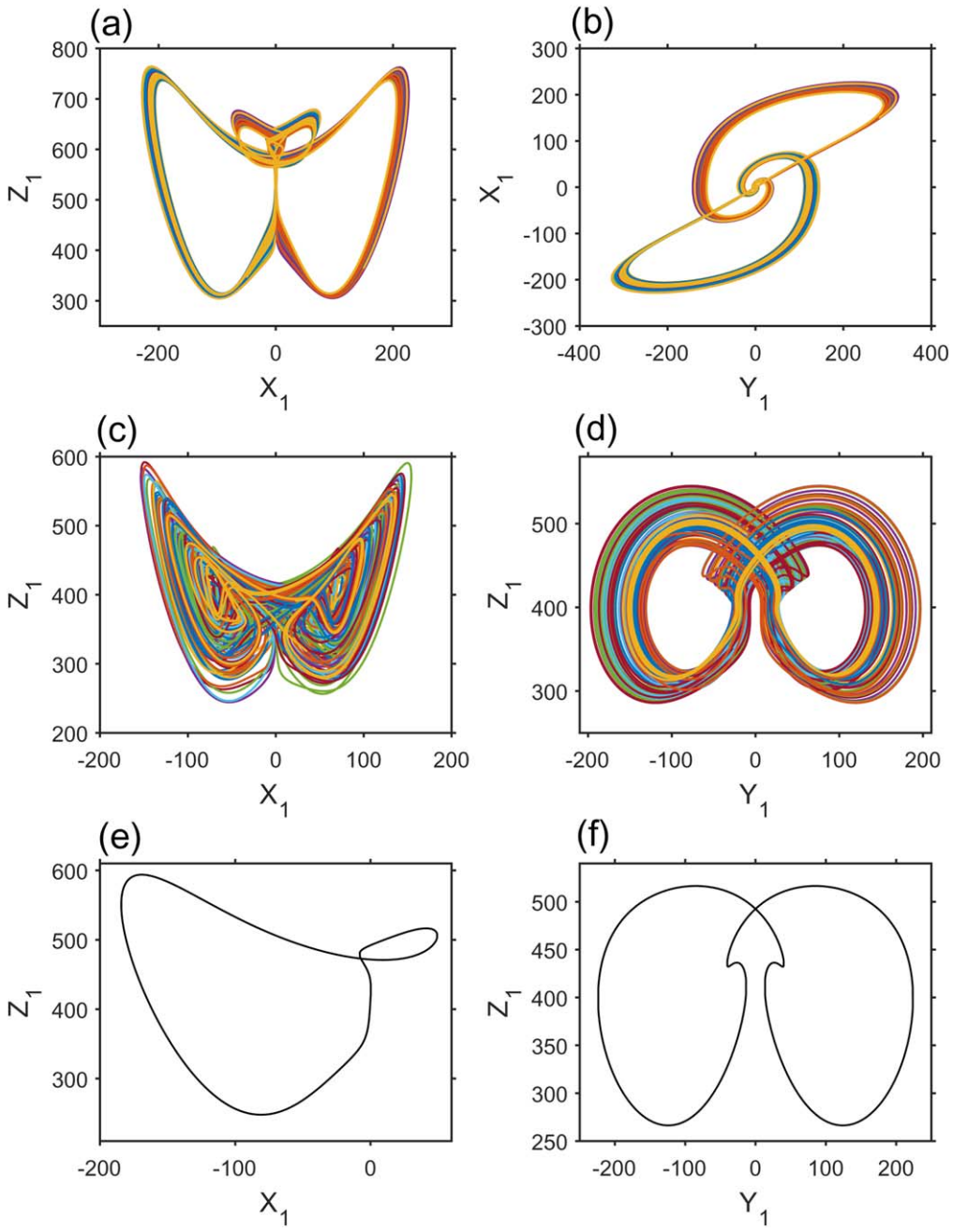

Figure 3. Trajectories of chaotic solutions for the 11-dimensional system with $r = 500$ and $\sigma = 101$ projected on (a) the X_1-Z_1 plane and (b) the Y_1-X_1 plane. Trajectories of chaotic solutions for (c) the 12-dimensional system with $r = 400$ and $\sigma = 40$ and (d) the 8-dimensional system with $r = 400$ and $\sigma = 70$. Trajectories of 2-periodic solutions for (e) the 11-dimensional system with $r = 400$ and $\sigma = 100$ and (f) the 23-dimensional system with $r = 400$ and $\sigma = 100$.

much insight regarding atmospheric predictability and uncertainty-mitigating strategies in modeling have been derived from direct and indirect applications of the Lorenz and Lorenz-like systems [30, 31]. In this view, high-dimensional Lorenz systems are not only interesting for their increased complexity in the equations and feedback loops but also as one way to conceptually examine the dependency of predictability on the system's ability to resolve smaller-scale motions.

Taking the Lorenz system as a conceptual model of fluid convection or numerical weather prediction, raising the dimension of the system via inclusion of additional Fourier modes is akin to refining the model resolution so that the model can capture smaller-scale motions; thus, extending the conclusions at the end of section 4, it can be suggested that the higher the resolution of a numerical model, the narrower becomes the range of parameters with which predictability of the model is hindered by the presence of chaos. Note that it is not unreasonable to have a fixed window of available parameters, even considering that the physical parameters vary in a model. For instance, both the Rayleigh parameter and the Prandtl number carry physical interpretations relevant to

thermal convection and are thus limited by physical reality. Predictability, in the sense of how likely the solution is to exhibit chaos, can then be said to improve with raising the dimension of the system.

Nonetheless, there exist several other notions of predictability that can be discussed in the context of the Lorenz system [32], the most typical of which is the limited predictability caused by the system's sensitivity to initial conditions. Indeed, the cornerstone argument against the possibility of having the perfect weather forecast in [2] is that in a chaotic model like the Lorenz system, tiny errors in the initial condition, which are unavoidable in practice due to observation errors, can result in a substantial difference in the solutions. In operational weather forecasting, this problem of rapid divergence of chaotic solutions is reflected in a practice called ensemble forecasting for which multiple forecasts are made to accommodate a probability distribution of future events, rather than producing a single numerically predicted weather [33, 34].

Going back to the Lorenz system, if we accept positive Lyapunov exponents as a signature of chaos [35], then a tiny difference in the initial condition is expected to grow exponentially in a chaotic solution. Suppose that a tiny perturbation is applied to the initial condition in an experiment in which the error between the original and perturbed solutions is tracked through integration time. It follows that after some time, the perturbed solution severely deviates from the original so that the error exceeds a certain threshold value. Once this threshold value is chosen, one can find the time that marks the first instance of the error exceeding this threshold. Denote this deviation time by τ_d, which is sometimes called the 'limit of deterministic predictability' or the 'predictability limit' in the context of numerical weather prediction [34]. Evidently there is a close relationship between τ_d and predictability. If τ_d is small, meaning the two solutions diverge rather quickly, then predictability can be said to be low and vice versa. The question we ask is this: does predictability in the sense of large τ_d improve in higher-dimensional systems? On the one hand, it is plausible that a system that accounts for more Fourier modes would produce results that are more precise or accurate; on the other hand, raising the dimension entails complicating the equation system, and more nonlinear terms are introduced with each step toward higher dimensions as shown in figure A2, which can make the solutions' behavior more unpredictable. Continuing with the weather forecasting example, this is akin to asking whether predictability in this sense improves in models with higher resolutions, in other words, if we can delay the so-called butterfly effect [36] purely by refining the model resolution.

The answer to that question according to the results of numerical experiments using the generalized Lorenz systems seems to be 'not always'. A sample of such results are displayed in figure 5. Here, the control initial condition is given by $(X_1, Y_1, Z_1, \ldots) = (1, 0, 0, \ldots)$ for each system and the perturbed initial condition is given by adding 10^{-4} to the initial condition for X_1. This small perturbation in the initial condition for X_1 leads to the difference exceeding 10.0 in magnitude at time τ_d in the solutions for Z_1 between the control and the perturbed. This difference magnitude of 10.0 was chosen to be a suitable value for determining the deviation time τ_d by trial and error. For example, our test results indicate that any threshold value $\gtrsim$0.58 can be chosen for this purpose when $r = 500$ and $\sigma = 50$ due to the sudden nature of deviation in these systems. Figures 5(a) and (b) show the τ_d computed in this way as a function of dimension, and figures 5(c)–(h) show for selected dimensions the time series of the control, the perturbed, and the absolute difference between the two from the experiments corresponding to figure 5(a). We see in figure 2(d) that given the parameters $r = 500$, $\sigma = 50$, and $b = 8/3$ as in figure 5(a), the solutions with both the control and perturbed initial conditions are chaotic for all dimensions up to dimension 33, beyond which the 35-dimensional system produces a steady-state solution as shown in figure 5(h), and consequently, there is no difference between the control and the perturbed as both solutions converge to the same fixed point. Raising the dimension of

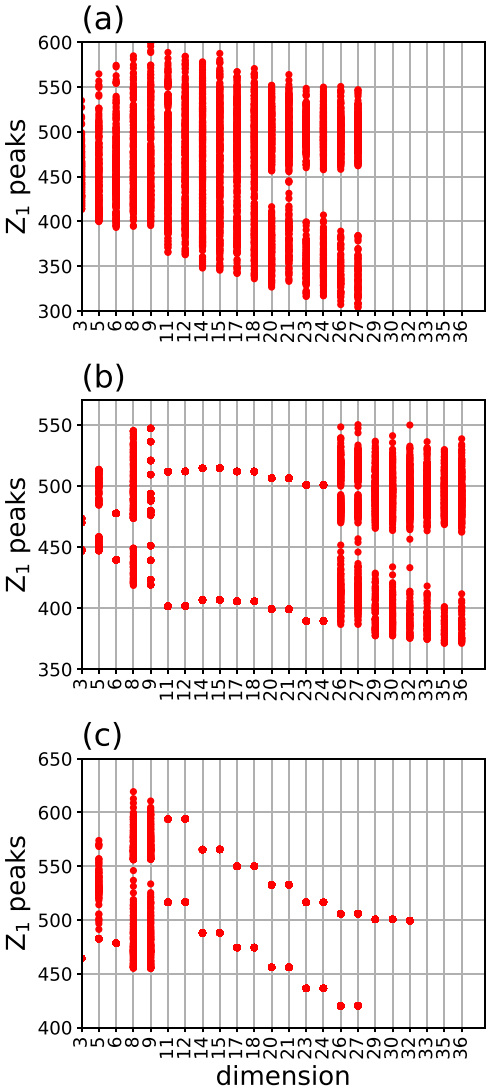

Figure 4. Bifurcation diagram across the dimensions: i.e. all peak Z_1-values found in the time series in $\tau \in [200, 230]$ of the solutions for the generalized Lorenz systems with dimensions ranging from 3 to 36 given $r = 400$ and (a) $\sigma = 40$, (b) $\sigma = 70$, and (c) $\sigma = 100$.

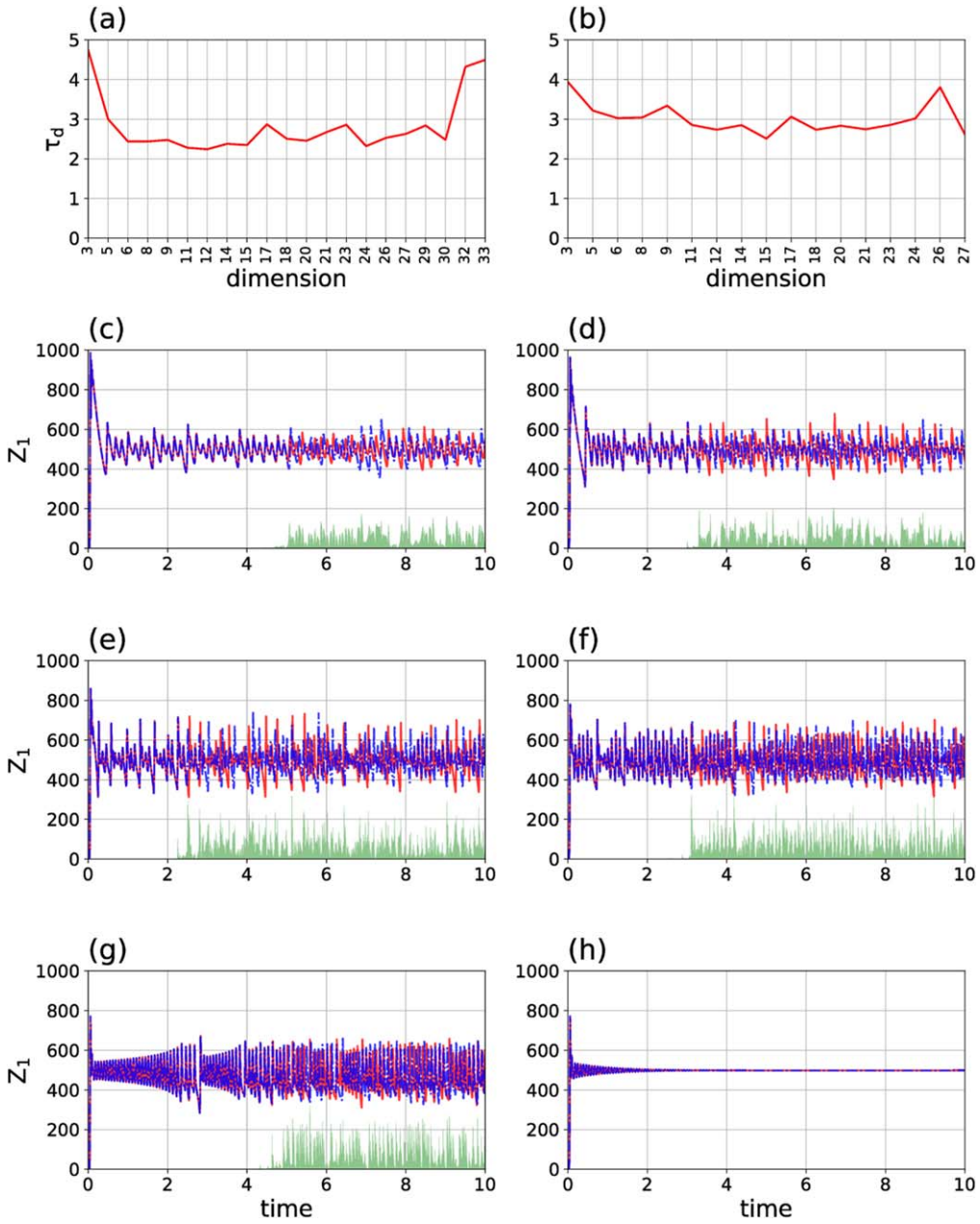

Figure 5. Sample of results from the initial condition experiments. The times at which the magnitude of the difference in the numerical solutions for Z_1 between the control and perturbed initial conditions exceeds the tolerance of 10 are plotted as a function of dimension in (a) with parameters $r = 500$ and $\sigma = 50$ and (b) with parameters $r = 400$ and $\sigma = 40$. The time series demonstrating the deviation of the two solutions (blue dashed-dot lines for the control and solid red for the perturbed) with the same parameters given for figure 5(a), solving the generalized Lorenz system of dimension (c) 3, (d) 5, (e) 12, (f) 17, (g) 32, and (h) 35. The green-shaded parts represent the absolute difference between the control and the perturbed solutions.

the system from 3 to 33, there is initially a dip in τ_d, which implies a quicker divergence between the two solutions and therefore poorer predictability. Predictability in this sense does not see any significant improvement until dimension hits 32, where τ_d is restored to the level comparable to that of the three-dimensional system. Still, the statement above applies only to this particular parameter combination used to plot figure 5(a). Under different (σ, r) choices, predictability evolves differently with dimension and there does not seem to be a conclusive pattern to this with respect to the dimension of the system. For example, given $r = 400$, $\sigma = 40$, and $b = 8/3$, shown in figure 5(b), predictability never recovers from the first blow from dimension 3 to dimensions 5 and 6, even though there appears to be a brief uptick at dimension 26. So long as chaos emerges, which is dictated by the initial condition and parameters, the dimension of the Lorenz system does not appear to have any consistent effect on predictability in this sense.

A robust confirmation of the above results requires analyzing the changes in deviation time τ_d across a variety of dimension-parameter combinations. To capture the broad patterns of predictability in dimension-parameter spaces,

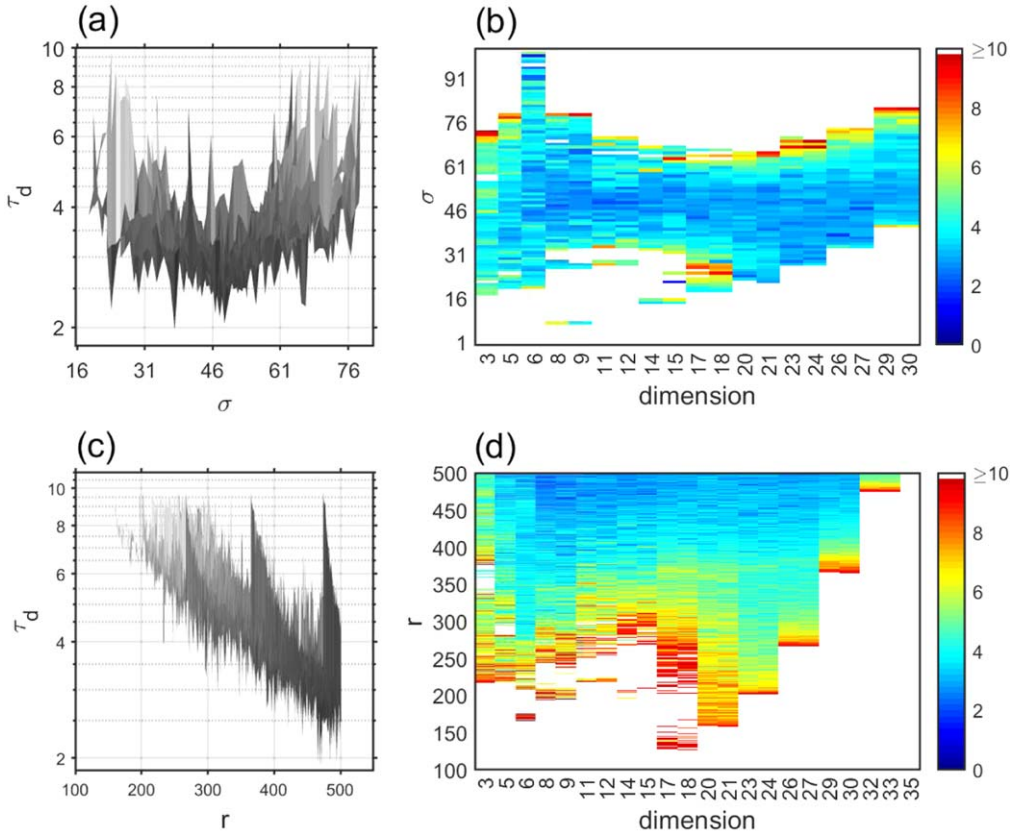

Figure 6. Deviation time (a) as a function of σ in a 3D rendering of the τ_d plot and (b) in the dimension-σ space, along the first band of chaos with $r = 500$ from figure 2(d). Deviation time (c) as a function of r in a 3D rendering of the τ_d plot and (d) in the dimension-r space, with $\sigma = 50$ corresponding to figure 2(b).

deviation times τ_d are plotted as a function of dimension and parameters in figure 6. Fixing $r = 500$, the dimension-σ plot in figure 6(b) clearly reveals the first band of chaos from figure 2(d). A sharp break in τ_d observed along $\tau_d \sim 10$ is associated with the boundaries between chaotic and non-chaotic regions. Figure 6(a) shows a 3D rendering of figure 6(b) from a perspective, whose valley-like pattern along σ suggests that the σ-dependency of τ_d is not monotonic. Overall, τ_d tends to be relatively small at the inner core of the chaotic band. Accordingly, it can be seen that the solutions are more unpredictable deeper inside the chaotic region which is in alignment with previously made observations [6]. From a physical point of view, however, the Prandtl number is not likely to exhibit high variabilities in the context of fluid convection, especially if the inherent characteristics of the fluid under consideration are not changed; rather, it is the Rayleigh parameter r that tends to greatly affect stability in fluid convection problems. The r-dependency is thus shown with σ fixed as 50 in figures 6(c) and (d). Again, the τ_d limit of 10 in figure 6 tends to capture the boundary between chaotic and non-chaotic regions from figure 2(b). The r-dependency shown in figure 6(c) suggests that τ_d tends to be lower when r is increased, which is reasonable since a higher r is generally associated with greater instability in fluid convection.

The analyses above show that raising the dimension in a chaotic system does not always lead to improved predictability despite being able to resolve smaller-scale motions. It is also notable that not only is τ_d a surprisingly reliable tool for detecting chaos, it can also serve as a robustness measure of a chaotic system, that is, how much chaos can withstand slight perturbations in the parameters, not unlike the Lyapunov exponents used for detecting different types of chaos [18]. Further development of this concept may also lead to a viable and cheaper alternative to Lyapunov vectors [37] or bred vectors [38] for artificially constructing ensemble members in numerical weather prediction. A low τ_d seems to be associated with how deeply embedded the particular parameter combination is in a chaotic region of the parameter space. It follows that depending on where the parameters are located within a chaotic region, an incremental change in dimension can improve or deteriorate predictability by bringing the system closer to or farther away from the boundary against non-chaotic regions.

6. Summary and discussion

This study generalizes the classic three-dimensional Lorenz system to the $(3N)$- and $(3N + 2)$-dimensional systems via selection of additional modes in the Fourier series expansions that appear in the derivation. Being able to produce a high-dimensional Lorenz system of any arbitrary dimension $(3N)$ or $(3N + 2)$, the generalizations allow for examining whether

the observed behavior of high-dimensional Lorenz systems in [6] continues as dimension is further raised.

The overall increase in the critical Rayleigh parameter beyond which the Lorenz attractor emerges continues indefinitely with rising dimensions. The collapsing of the onion-like structure observed in some high-dimensional systems [6] also continues beyond dimension 11, although the collapsing stops short of destroying altogether the first and second bands of chaos in the σ-space. In fact, there appears a shifting of the second band of chaos towards larger σ shown as a step function-like pattern in the dimension-σ periodicity diagrams. The expansion of the periodic region in high-dimensional systems seen in [6] does not continue. On the contrary, the periodic regions also start disappearing leading to the eventual end of instability when dimension is sufficiently high. These observations, together with time series analyses, lead to our discussion of predictability.

Two notions of predictability concerning the Lorenz system are discussed. First, we take the area of the chaotic region appearing within the fixed window of a parameter space as a means to assessing predictability. In both dimension-r and dimension-σ periodicity diagrams, the region in which the numerical solutions are unstable, which includes chaos, seems to shrink and eventually disappear with rising dimensions. Predictability according to the first notion can, therefore, be said to generally improve with an increase in the dimension of the Lorenz system. The second notion of predictability is based on the solutions' sensitivity to initial conditions. Comparing the time series of two numerical solutions, one with the control initial condition and the other with a slightly perturbed initial condition, the time τ_d at which the perturbed solution significantly deviates from the control solution marks the predictability limit. While the predictability limit does change from dimension to dimension, the effect of raising the dimension of the system seems to have effects in both directions depending on other factors involved. The role played by the dimension of the system alone in relation to predictability according to the second notion still remains elusive.

It is noted that there is still too big of a gap between the Lorenz systems, even the high-dimensional ones, and other sophisticated numerical models that mimic natural phenomena more closely such as the models used for numerical weather prediction. For this reason, caution is required when applying the conclusions of this study about predictability to numerical predictions of weather and climate. Moreover, while many studies after [2] have since presumed or attempted to find potential links between strange attractors and natural phenomena such as turbulent flows [21, 22, 39, 40], it is still unclear how much of the chaotic characteristics found in the Lorenz systems reflect those found in nature [30, 41, 42]. We suspect that chaos exhibited by the Lorenz systems, numerical weather and climate predictions, and natural phenomena are interrelated, but still more research is needed either to clarify their relationships or to bridge the gaps between those three. Studying the changes brought about by increases in the dimension of the Lorenz system using generalizations such as the $(3N)$- and $(3N + 2)$-dimensional systems here can be a step in that direction.

Despite the limitations, it may still be possible to obtain some fundamental insights from studying these systems as conceptual models. For instance, our conclusions about predictability are to some extent both plausible and relevant to the current state of atmospheric modeling. Indeed, improving the model resolution should improve predictability to a certain degree, whereas it is also often acknowledged that having a finer resolution alone does not always lead to improved predictability.

In a future study, we plan to examine other aspects of the $(3N)$- and $(3N + 2)$-dimensional systems. One phenomenon to consider is self-synchronization [43], which is yet to be fully explored in high-dimensional Lorenz systems. In addition, other physically extended Lorenz-like systems such as the Lorenz-Stenflo system [11, 13] can also be generalized likewise, and exploring their potentially rich dynamics [44] can be of interest to many.

Acknowledgments

This work was supported by the Small Grant for Exploratory Research (SGER) program through the National Research Foundation of Korea (NRF) funded by the Ministry of Science and ICT (MSIT) (2018R1D1A1A02086007).

Appendix. Derivation

In the derivations below, the same notations used in [6] are adopted for consistency. Note that the generalized Lorenz systems studied here are formulated differently from that of [45], whose generalization focuses on appending additional nonlinear terms for the purpose of studying aggregated negative feedback loops.

Following [46], we start with the nondimensionalized governing equations for Rayleigh-Bénard convection in the x-z space as follows:

$$\frac{\partial \nabla^2 \psi}{\partial t} = \frac{\partial \psi}{\partial z}\frac{\partial \nabla^2 \psi}{\partial x} - \frac{\partial \psi}{\partial x}\frac{\partial \nabla^2 \psi}{\partial z} + \sigma \frac{\partial \theta}{\partial x} + \sigma \nabla^4 \psi, \tag{A.1}$$

$$\frac{\partial \theta}{\partial t} = \frac{\partial \psi}{\partial z}\frac{\partial \theta}{\partial x} - \frac{\partial \psi}{\partial x}\frac{\partial \theta}{\partial z} + \mathrm{Ra}\frac{\partial \psi}{\partial x} + \nabla^2 \theta, \tag{A.2}$$

where Ra is the Rayleigh number. Here, the time derivatives are taken with respect to t, which will later be replaced by the scaled time $\tau = \pi^2(1 + a^2)t$. Note that the Rayleigh parameter r in the three-dimensional Lorenz system [2] is defined by $\mathrm{Ra}/\mathrm{Ra}_c$ with Ra_c being the critical Rayleigh number for the Rayleigh-Bénard convection under consideration. In [6], the variables ψ and θ, which are referred to as the stream-function and the temperature perturbation, respectively, are approximated by truncation of the following series expansions:

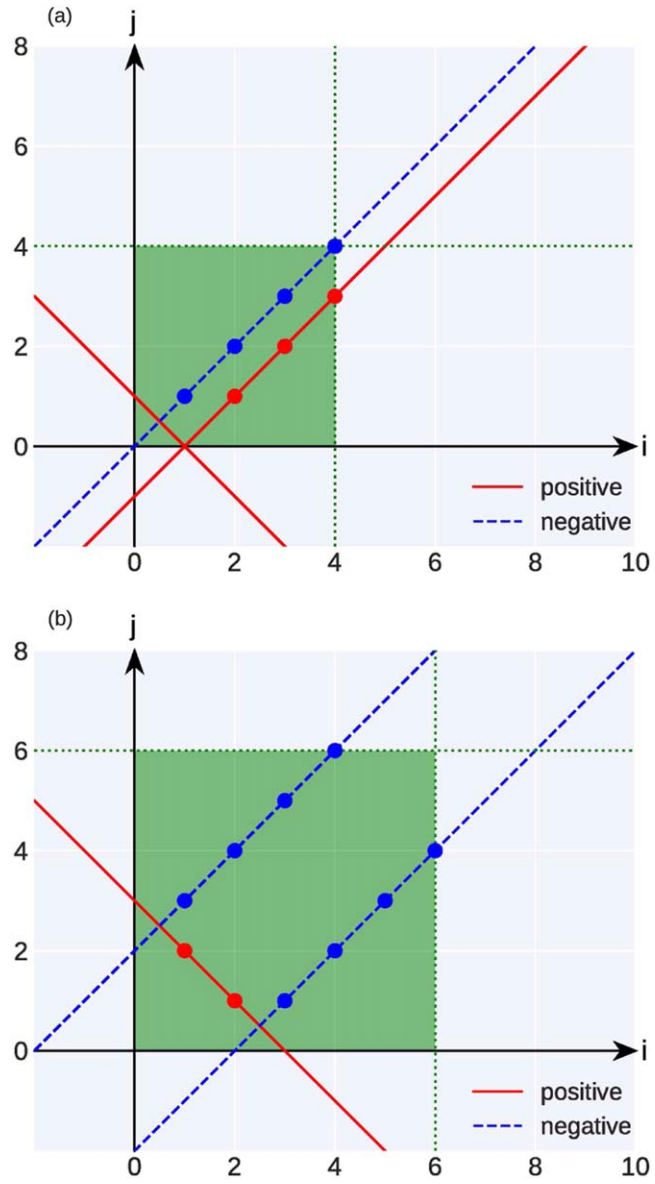

Figure A1. The filled circles indicate the index pairs (i, j) that belong to (a) the P_1-set corresponding to the nonlinear terms X_iZ_j included in the $\dot{Y}_1$ equation of the 12-dimensional system and (b) the Q_2-set corresponding to the nonlinear terms X_iY_j included in the $\dot{Z}_2$ equation of the 18-dimensional system. Along the red solid lines, the corresponding sign function, $\mathcal{S}_Y$ or $\mathcal{S}_Z$, is positive, and along the blue dashed lines, the sign functions are negative. The choice of pairs is bounded by the i-axis, j-axis, (i.e. there are no indices $\leqslant 0$) and the green dotted lines determined by the dimension and type of the system.

$$\psi \approx \frac{1+a^2}{a}\sum_{n=1}^{N}(X_n\sqrt{2}\,\sin(\pi a x)\sin((2n-1)\pi z)), \quad \text{(A.3)}$$

$$\theta \approx \frac{\pi^3(1+a^2)^3}{a^2}\sum_{m=1}^{M}(Y_m\sqrt{2}\,\cos(\pi a x)\sin((2m-1)\pi z) - Z_m\sin(2m\pi z)) \quad \text{(A.4)}$$

for constant $a = 1/\sqrt{2}$ and a choice of mode numbers $N, M \in \mathbb{Z}$, $N, M > 0$. The dimension of the resulting nonlinaer ODE system $(N + 2M)$, therefore, depends on how many modes are chosen to survive the truncations in (A.3) and (A.4). Following the derivation scheme used in [6], there are two different manifestations of this generalization, each leading to either a $(3N)$- or $(3N + 2)$-dimensional system depending on the respective choice of N and M. Setting $N = M$ leads to $(3N)$-dimensional ODE systems, whereas setting $M = N + 1$ yields $(3N + 2)$-dimensional systems. Note that in deriving the systems with dimensions 5, 6, 8, 9, and 11 in [6], the condition $0 \leqslant M - N \leqslant 1$ was imposed so that the dimension of the system would rise one step at a time.

A.1. Derivation of the (3*N*)*-dimensional generalization*

Reorganizing (A.1) after plugging in the Fourier series expansions of ψ and θ yields for each $m = n$,

$$\dot{X}_n = \frac{\sigma\pi^2(1+a^2)^2}{a^2+(2n-1)^2}Y_m - \sigma\pi^2(a^2+(2n-1)^2)X_n \quad \text{(A.5)}$$

$$= \frac{\sigma\pi^2(1+a^2)}{d_n}Y_m - d_n\sigma\pi^2(1+a^2)X_n, \quad \text{(A.6)}$$

where $d_n \equiv (a^2 + (2n - 1)^2)/(1 + a^2)$ and the dot above variable X denotes the derivative with respect to time t. Applying the substitution $\tau = \pi^2(1 + a^2)t$, we obtain (6) for each $k = n = m$ reproduced below:

$$\dot{X}_k = \frac{\sigma}{d_k}Y_k - d_k\sigma X_k. \quad \text{(A.7)}$$

Note that the dot above variable X now denotes the derivative with respect to τ.

The $\dot{Y}_k$ and $\dot{Z}_k$ equations are obtained by selectively combining the appropriate terms in (A.4) and decoupling it into two equations (A.8) and (A.9) as follows:

$$\begin{aligned}
&\frac{\pi^3(1+a^2)^3}{a^2}\sum_{m=1}^{M}(\dot{Y}_m\sqrt{2}\,\cos(\pi a x)\sin((2m-1)\pi z))\\
&= -\frac{1+a^2}{a}\sum_{n=1}^{N}(X_n\sqrt{2}\,\pi a\cos(\pi a x)\sin((2n-1)\pi z))\\
&\times\frac{\pi^3(1+a^2)^3}{a^2}\sum_{m=1}^{M}(-2Z_m m\pi\cos(2m\pi z))\\
&+\mathrm{Ra}\frac{1+a^2}{a}\sum_{n=1}^{N}(X_n\sqrt{2}\,\pi a\cos(\pi a x)\sin((2n-1)\pi z))\\
&-\frac{\pi^3(1+a^2)^3}{a^2}\sum_{m=1}^{M}(Y_m\sqrt{2}\,\pi^2a^2\cos(\pi a x)\sin((2m-1)\pi z))\\
&-\frac{\pi^3(1+a^2)^3}{a^2}\\
&\times\sum_{m=1}^{M}(Y_m\sqrt{2}\,(2m-1)^2\pi^2\cos(\pi a x)\sin((2m-1)\pi z))
\end{aligned} \quad \text{(A.8)}$$

and

$$\begin{aligned}
&\frac{\pi^3(1+a^2)^3}{a^2}\sum_{m=1}^{M}(-\dot{Z}_m\sin(2m\pi z))\\
&=\frac{1+a^2}{a}\sum_{n=1}^{N}(X_n\sqrt{2}\,(2n-1)\pi\sin(\pi ax)\cos((2n-1)\pi z))\\
&\times\frac{\pi^3(1+a^2)^3}{a^2}\sum_{m=1}^{M}(-Y_m\sqrt{2}\sin(\pi ax)\sin((2m-1)\pi z))\pi a\\
&-\frac{1+a^2}{a}\sum_{n=1}^{N}(X_n\sqrt{2}\,\pi a\cos(\pi ax)\sin((2n-1)\pi z))\\
&\times\frac{\pi^3(1+a^2)^3}{a^2}\\
&\times\sum_{m=1}^{M}(Y_m\sqrt{2}\,(2m-1)\pi\cos(\pi ax)\cos((2m-1)\pi z))\\
&+\frac{\pi^3(1+a^2)^3}{a^2}\sum_{m=1}^{M}(4Z_m m^2\pi^2\sin(2m\pi z)).
\end{aligned}\tag{A.9}$$

Note that the terms inside the standalone sums can be separated by specifying n and m, while the matter is a bit more complicated for the sums multiplied together. The crux of our derivation is in choosing the appropriate nonlinear terms that are to be included in each equation corresponding to a specific n or m so that all terms can be collapsed under the sinusoidal functions with a matching wavenumber as demonstrated in figure A1.

In the case of (A.8), the terms specific to $\dot{Y}_k$, where k can either be n or m, are extracted as follows:

$$\begin{aligned}
&\frac{\pi^3(1+a^2)^3}{a^2}\sqrt{2}\cos(\pi ax)\sin((2k-1)\pi z)\dot{Y}_k\\
&=\mathrm{Ra}\frac{1+a^2}{a}\sqrt{2}\,\pi a\cos(\pi ax)\sin((2k-1)\pi z)X_k\\
&\quad-\frac{\pi^3(1+a^2)^3}{a^2}\sqrt{2}\,\pi^2\cos(\pi ax)\sin((2k-1)\pi z)\\
&\quad\times(a^2+(2k-a)^2)Y_k\\
&\quad+\left(\frac{1+a^2}{a}\right)\frac{\pi^3(1+a^2)^3}{a^2}2\sqrt{2}\,\pi^2 a\\
&\quad\times\cos(\pi ax)[\Sigma_1]_{\omega=2k-1}[\Sigma_2]_{\omega=2k-1}.
\end{aligned}\tag{A.10}$$

Here, ω is the wavenumber for the sinusoidal expressions within the sums Σ_1 and Σ_2, which are defined by

$$\begin{aligned}
\Sigma_1=&X_1\sin(\pi z)+X_2\sin(3\pi z)\\
&+\cdots+X_N\sin((2N-1)\pi z)
\end{aligned}\tag{A.11}$$

and

$$\begin{aligned}
\Sigma_2=&Z_1\cos(2\pi z)+2Z_2\cos(4\pi z)\\
&+\cdots+MZ_M\cos(2M\pi z),
\end{aligned}\tag{A.12}$$

so that only the terms satisfying the condition $\omega=2k-1$ survives the filter $[\cdot]_{\omega=2k-1}$ in (A.10). The unfiltered product $\Sigma_1\Sigma_2$ can be rewritten via the following trigonometric identity,

$$\begin{aligned}
&\sum_{n=1}^{N}\sum_{m=1}^{M}mX_nZ_m\sin((2n-1)\pi z)\cos(2m\pi z)\\
&=\sum_{n=1}^{N}\sum_{m=1}^{M}\frac{m}{2}X_nZ_m(\sin((2m+2n-1)\pi z)\\
&\quad-\sin((2m-(2n-1))\pi z)),
\end{aligned}\tag{A.13}$$

through which passing the filter $\omega=2k-1$ comes down to satisfying one of the following conditions:

$$\begin{cases}n+m=k,\\ m-n=k-1,\\ n-m=k.\end{cases}\tag{A.14}$$

Note that the condition $m+n=1-k$ is not needed since $m+n>1$ and $n>0$. Then the n and m satisfying one of the three conditions in (A.14) form a set of integer pairs $P_k\subset\{(n,m)|n\leqslant N,\ m\leqslant M\}$ as defined in section 2.1:

$$P_k\equiv\{(i,j)\colon i+j=k\ \text{or}\ j-i=k-1\ \text{or}\ i-j=k\}.\tag{A.15}$$

To avoid confusion, the indices n and m satisfying (A.14) are denoted by i and j, respectively. Note that -1 survives when the second sinusoidal term on the right-hand-side of (A.13) passes the ω-filter. To address this, we introduce a sign function $\mathcal{S}_Y$ that becomes negative when $j-i=k-1$ is satisfied. Reorganizing (A.10) and applying the substitutions

$$\begin{aligned}
&d_k=\frac{(2k-1)^2+a^2}{1+a^2},\quad \tau=\pi^2(1+a^2)t,\\
&\mathrm{Ra}_c=\frac{\pi^4}{a^2}(1+a^2)^3,\quad\text{and}\quad r=\frac{\mathrm{Ra}}{\mathrm{Ra}_c},
\end{aligned}\tag{A.16}$$

we get (7) reproduced below:

$$\dot{Y}_k=rX_k-d_kY_k+\sum_{(i,j)\in P_k}(jX_iZ_j\mathcal{S}_Y).\tag{A.17}$$

In the case of (A.9), the terms specific to $\dot{Z}_k$ are extracted as follows:

$$\begin{aligned}
&\frac{\pi^3(1+a^2)^3}{a^2}(-\dot{Z}_k\sin(2k\pi z))\\
&=-\frac{1+a^2}{a}\sqrt{2}\,\pi\sin(\pi ax)\frac{\pi^3(1+a^2)^3}{a^2}\\
&\quad\times\sqrt{2}\sin(\pi ax)\pi a[\Pi_1]_{|\omega|=2k}\\
&\quad-\frac{1+a^2}{a}\sqrt{2}\,\pi a\cos(\pi ax)\frac{\pi^3(1+a^2)^3}{a^2}\\
&\quad\times\sqrt{2}\,\pi\cos(\pi ax)[\Pi_2]_{|\omega|=2k}\\
&\quad+\frac{\pi^3(1+a^2)^3}{a^2}Z_k4k^2\pi^2\sin(2k\pi z).
\end{aligned}\tag{A.18}$$

Here, the products Π_1 and Π_2 defined by

$$\begin{aligned}
\Pi_1=&\sum_{n=1}^{N}(X_n\cos((2n-1)\pi z)(2n-1))\\
&\times\sum_{m=1}^{M}(Y_m\sin((2m-1)\pi z))
\end{aligned}\tag{A.19}$$

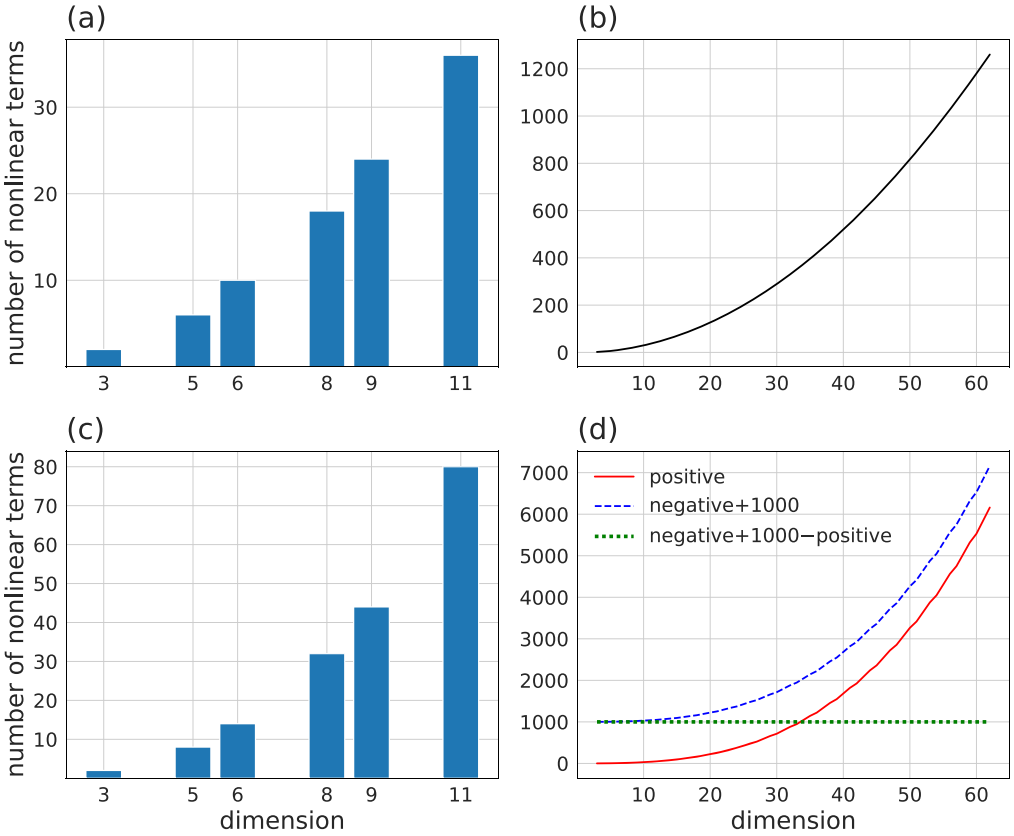

Figure A2. The number of nonlinear terms as a function of the dimension of the system (a)–(b) not accounting for the coefficients and (c)–(d) taking into account the coefficients. Note that (d) shows the number of nonlinear terms with positive and negative coefficients separately and 1000 is added to the number of nonlinear terms with negative coefficients in order to compare the two curves.

and

$$\Pi_2 = \sum_{n=1}^{N}(X_n \sin((2n-1)\pi z)) \times \sum_{m=1}^{M}(Y_m(2m-1)\cos((2m-1)\pi z)) \tag{A.20}$$

contain the nonlinear terms and the sinusoidal functions that ought to be filtered by the wavenumber $\omega = 2k$ or $\omega = -2k$ so that these terms can be collapsed under the banner of a single sinusoidal function, $\sin(2k\pi z)$. Applying trigonometric identities, we have

$$\begin{aligned}\Pi_1 &= \sum_{n=1}^{N}\sum_{m=1}^{M}(2n-1)X_nY_m \times \sin((2m-1)\pi z)\cos((2n-1)\pi z) \\ &= \frac{1}{2}\sum_{n=1}^{N}\sum_{m=1}^{M}(2n-1)X_nY_m(\sin((2m+2n-2)\pi z) + \sin((2m-2n)\pi z)).\end{aligned} \tag{A.21}$$

Filtering of the sinusoidal terms in (A.21) can be done through the choices of appropriate X_i and Y_j, whose index pairs belong in the set $Q_{k,1}$ defined by

$$Q_{k,1} \equiv \{(i,j)\colon j + i = k+1 \text{ or } |j-i| = k\}. \tag{A.22}$$

Again to avoid confusion, the indices corresponding to $n \leqslant N$ and $m \leqslant M$ satisfying (A.22) are denoted by i and j, respectively. The associated sign function $\mathcal{S}_{Z,1}$ is given so that it is negative if $i - j = k$. Note that the condition $j + i = 1 - k$ needs not be included in the definition as $i + j > 1$ and $1 - k < 1$ for all possible i, j, and k. Likewise, applying trigonometric identities to Π_2 yields

$$\Pi_2 = \frac{1}{2}\sum_{n=1}^{N}\sum_{m=1}^{M}(2m-1)X_nY_m(\sin((2m+2n-2)\pi z) - \sin((2m-2n)\pi z)), \tag{A.23}$$

which leads to the set $Q_{k,2}$ of nonlinear index pairs (i,j) satisfying the condition $|i-j| = k$. The associated sign function $\mathcal{S}_{Z,2}$ for the terms from Π_2 turns negative when $j - i = k$. Let $Q_k \equiv Q_{k,1} \cup Q_{k,2}$ and combine the definitions for $\mathcal{S}_{Z,1}$ and $\mathcal{S}_{Z,2}$ to define $\mathcal{S}_Z$ so that it turns negative when either of the conditions $j - i = k$ and $i - j = k$ is satisfied. Applying the substitutions $b = 4/(1+a^2)$ and $\tau = \pi^2(1+a^2)t$, we obtain (8) for the $\dot{Z}_k$ equation reproduced below:

$$\dot{Z}_k = -k^2bZ_k + \sum_{(i,j)\in Q_k}(kX_iY_j\mathcal{S}_Z). \tag{A.24}$$

A.2. Derivation of the (3N+2)-dimensional generalization

The derivation of the $(3N + 2)$-dimensional system closely follows that of the $(3N)$-dimensional system, except now we also consider the case when $m \neq n$ in (A.3) and (A.4). Because of the imposed condition $0 \leqslant M - N \leqslant 1$, if $m \neq n$ is allowed, then the system now includes two extra equations with $\dot{Y}_{N+1}$ and $\dot{Z}_{N+1}$ in addition to $3N$ equations with $\dot{X}_k$, $\dot{Y}_k$, and $\dot{Z}_k$ for $k = 1, \ldots, N$. Note that $\dot{Y}_{N+1}$ equation differs from the other $\dot{Y}_k$ equations with $k < N + 1$ in that it does not contain the X_{N+1} term. Furthermore, despite having the same form in both dimension-type systems, (10) and (11) for $k \leqslant N$ in the $(3N + 2)$-dimensional systems have more terms than (7) and (8) in the $(3N)$-dimensional systems. This is because the choice of (i,j)-pairs in the P_k- and Q_k-sets depends not only on N but also on M, which matters when $N \neq M$.

A.3. Choosing the nonlinear pairs

The definitions of the sets P_k and Q_k are at the heart of our generalization because they dictate which pairs of variables are multiplied together to introduce nonlinearity to the ODE systems. As the definitions suggest, the choice of nonlinear index pairs in each equation of the generalized system comes down to its indices satisfying one of the prescribed conditions. This process is illustrated in figure A1 for specific k and dimension numbers.

The number of nonlinear terms accumulated in this way increases dramatically as shown in figures A2(a) and (b). A similar increase in the number of nonlinear terms is seen when the counting takes into account the coefficients so that, for example, $-3X_2Y_3$ is counted three times (figure A2(c)). Figure A2(d) reveals that if the counting takes into account the coefficients, then regardless of the dimension of the system the number of nonlinear terms with positive coefficients is equal to that with negative coefficients.

ORCID iDs

Jong-Jin Baik https://orcid.org/0000-0003-3709-0532

References

[1] Tucker W 1999 *Comptes Rendus de l'Académie des Sciences–Series I–Mathematics* **328** 1197–202
[2] Lorenz E N 1963 *J. Atmos. Sci.* **20** 130–41
[3] Musielak Z E and Musielak D E 2009 *Int. J. Bifurcation Chaos* **19** 2823–69
[4] Curry J H 1978 *Commun. Math. Phys.* **60** 193–204
[5] Shen B W 2014 *J. Atmos. Sci.* **71** 1701–23
[6] Moon S, Han B S, Park J, Seo J M and Baik J J 2017 *Int. J. Bifurcation Chaos* **27** 1750176
[7] Veronis G 1968 *J. Fluid Mech.* **34** 315–36
[8] Veronis G 1968 *J. Fluid Mech.* **31** 113–39
[9] Moore D R, Toomre J, Knobloch E and Weiss N O 1983 *Nature* **303** 663–7
[10] Bhattacharjee J K and McKane A J 1988 *J. Phys. A: Math. Gen.* **21** L555–8
[11] Stenflo L 1996 *Phys. Scr.* **53** 83–4
[12] Macek W M 2018 *Nonlinear Dyn.* **94** 2957–68
[13] Moon S, Seo J M, Han B S, Park J and Baik J J 2019 *Chaos* **29** 063129
[14] Rossler O E 1979 *Phys. Lett.* **71A** 155–7
[15] Peng J H, Ding E J, Ding M and Yang W 1996 *Phys. Rev. Lett.* **76** 904–7
[16] Reiterer P, Lainscsek C, Schürrer F, Letellier C and Maquet J 1998 *J. Phys. A: Math. Gen.* **31** 7121–39
[17] Rech P C 2016 *Phys. Scr.* **91** 125201
[18] Rech P C 2017 *Eur. Phys. J.* B **90** 251
[19] Park J, Lee H, Jeon Y L and Baik J J 2015 *Phys. Scr.* **90** 065201
[20] Yorke J A and Yorke E D 1979 *J. Stat. Phys.* **21** 263–77
[21] Sparrow C 1982 *The Lorenz equations: Bifurcations, Chaos, and Strange Attractors* (New York: Springer)
[22] Kaplan J L and Yorke J A 1979 *Commun. Math. Phys.* **67** 93–108
[23] Shen B W 2015 *Nonlinear Processes Geophys.* **22** 749–64
[24] Afraimovich V S, Bykov V V and Shilnikov L P 1977 *Soviet Physics Doklady* **22** 253–5
[25] Bykov V V and Shilnikov L P 1992 *Sel. Math. Sov.* **11** 375–82
[26] Barrio R and Serrano S 2007 *Physica* D **229** 43–51
[27] Dullin H R, Schmidt S, Richter P H and Grossmann S K 2007 *Int. J. Bifurcation Chaos* **17** 3013–33
[28] Creaser J L, Krauskopf B and Osinga H M 2017 *SIAM Journal of Applied Dyanamical Systems* **16** 2127–64
[29] Rech P C 2015 *Phys. Scr.* **90** 115201
[30] McWilliams J C 2019 *Earth and Space Science* **6** 336–50
[31] Yoden S 2007 *Journal of the Meteorological Society of Japan* **85B** 77–102
[32] Chu P C 1999 *J. Atmos. Sci.* **56** 1427–32
[33] Palmer T N 2002 *Q. J. R. Meteorolog. Soc.* **128** 747–74
[34] Lewis J M 2005 *Mon. Weather Rev.* **133** 1865–85
[35] Wiggins S 2003 *Introduction to Applied Nonlinear Dynamical Systems and Chaos* 2nd edn (New York: Springer)
[36] Palmer T N, Döring A and Seregin G 2014 *Nonlinearity* **27** R123–41
[37] Feng J, Ding R and Liu D 2014 *J. Atmos. Sci.* **71** 3554–67
[38] Toth Z and Kalnay E 1997 *Mon. Weather Rev.* **125** 3297–319
[39] Ruelle D and Takens F 1971 *Commun. Math. Phys.* **20** 167–92
[40] Gollub J P and Swinney H L 1975 *Phys. Rev. Lett.* **35** 927–30
[41] Crutchfield J P and Kaneko K 1988 *Phys. Rev. Lett.* **60** 2715–8
[42] Ghil M 2019 *Earth and Space Science* **6** 1007–42
[43] Pecora L M and Carroll T L 1990 *Phys. Rev. Lett.* **64** 821–4
[44] Park J, Han B S, Lee H, Jeon Y L and Baik J J 2016 *Phys. Scr.* **91** 065202
[45] Shen B W 2019 *Int. J. Bifurcation Chaos* **29** 1950037
[46] Saltzman B 1962 *J. Atmos. Sci.* **19** 329–41